Applied Food Research 3 (2023) 100250

Contents lists available at ScienceDirect

Applied Food Research

journal homepage: www.elsevier.com/locate/afres

Characterization of vasskveite (water halibut) syndrome for automated detection

Samuel Ortega[a], Ragni Ofstad[b], Shaheen Syed[a], Mathias Kranz[c,d], Karsten Heia[a], Kathryn E. Anderssen[a,*]

[a] Department of Seafood Industry, Nofima AS, P.O. Box 6122, Tromsø 9291, Norway
[b] Department of Food Science, Nofima AS, P.O. Box 6122, Tromsø 9291, Norway
[c] PET Imaging Center Tromsø, University Hospital North-Norway (UNN), Tromsø 9009, Norway
[d] Nuclear Medicine and Radiation Biology Research Group, the Arctic University of Norway, UiT, Tromsø 9009, Norway

ARTICLE INFO

Keywords:
Fish
Halibut
Hyperspectral imaging
Magnetic resonance imaging
Quality control
Vasskveite
Mushy halibut syndrome

ABSTRACT

In recent years, cases of vasskveite (water halibut) syndrome in halibut have been increasing. At the moment, there exists no way to screen for the syndrome immediately after capture, which is problematic for both exporters and purchasers. In this article, we compared good quality halibut and halibut exhibiting the syndrome using a variety of techniques. Hyperspectral imaging was used to quantify the relative amounts of fat and water in the tissue. Diffusion tensor imaging was used to characterize tissue structure. Histology was performed to provide direct visual characterization of the tissue. Results indicate the muscle fibers in afflicted fish exhibit disordered growth and the tissue is lacking in fat. These results are in line with the current theory that the syndrome stems from a nutritional deficiency in the halibut diet. Hyperspectral imaging appears to be a promising technology to rapidly identify afflicted halibut immediately after capture.

1. Introduction

Pacific halibut (*Hippoglossus stenolepis*) and Greenland halibut *(Reinhardtius hippoglossoides*) are important fish species for both commercial and recreational fishing ("Capture and Production by Species", 2017). For example, commercial landings of Pacific halibut in Alaska are valued at approximately 100 million USD per year while commercial landings of Greenland halibut in Canada are valued at approximately 90 million USD per year. While halibut flesh is typically translucent and firm, cases have been arising where some fillets have a soft, jelly-like texture and may be opaque in appearance. The flesh is visually unappealing, oozes water when cooked, and cannot be smoked, such that these fillets are undesirable for both consumers and producers. Afflicted halibut are referred to as "Vasskveite" (water halibut) due to the watery texture of the fish (Kvile, 2019). This syndrome has been noted as far back as 1989 in waters near Alaska and Greenland, where it has been dubbed "mushy halibut syndrome". However, cases appear to be on the rise in recent years, with instances now appearing in Iceland and Norway. Producers are fielding an increasing number of complaints and requests from exporters and customers for reduced pricing due to this poor-quality fish in the deliveries (Sandøy, 2019). Therefore, there is a great desire by producers to be able to screen fish for the syndrome at landing. However, at the moment, it is not possible to separate out the potentially afflicted fish right after capture, as the syndrome is only evident after they have come out of rigor mortis some days later. To date, it is difficult to know how widespread of a problem the syndrome is due to the lack of methods to efficiently screen for it. No publications on the syndrome exist in the scientific literature, although some information exists in state reports ("Mushy Halibut Syndrome", 2011). The syndrome is believed to arise not from bacteria or parasites, but from nutritional deficiencies of the fish. This affliction is different than "chalky halibut", which is caused by the buildup of lactic acid in the muscles of the fish due to extended struggling during capture.

In this article, we have two main goals. Firstly, we aim to better characterize the tissue to determine what causes the jelly like consistency. Secondly, we investigate the possibilities to provide rapid screening for the syndrome immediately after landing. To do this, we use several different characterization techniques to investigate both the chemistry and physical structure of the tissue. Histology was performed on both good and poor-quality samples to provide a visual overview of the tissue structure and composition. Another method is hyperspectral imaging (HSI). Regular cameras measure three wavelengths per pixel: one in the red re-

* Corresponding author.
E-mail address: kate.anderssen@nofima.no (K.E. Anderssen).

https://doi.org/10.1016/j.afres.2022.100250
Received 20 September 2022; Received in revised form 19 December 2022; Accepted 20 December 2022
Available online 23 December 2022

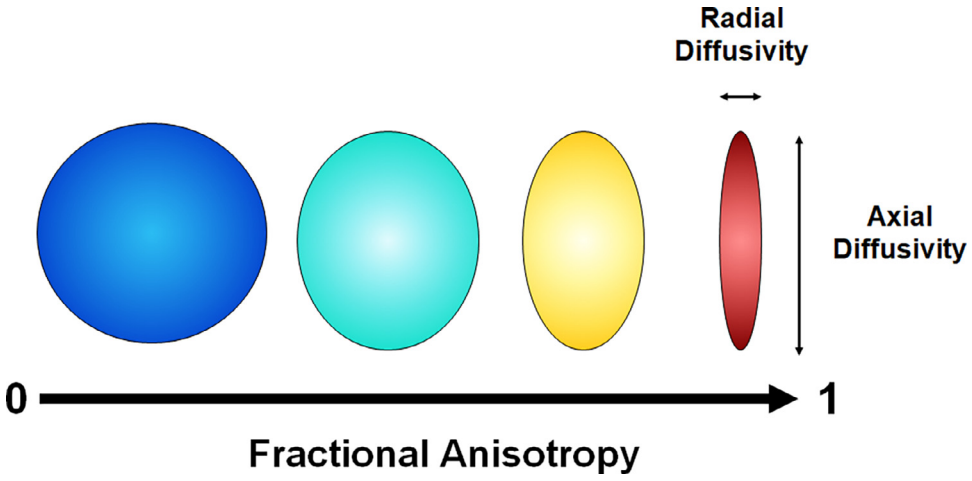

Fig. 1. Diffusion tensor imaging metrics.

gion of the visual light spectrum, one in the green region and one in the blue region. Hyperspectral cameras, on the other hand, measure numerous light wavelengths simultaneously. Depending on the camera, these may be in the visual light spectrum or may extend in to the ultraviolet or infrared (IR) regions of light. When a sample is measured with a hyperspectral camera, each pixel in the resulting image contains information about how light is transmitted and absorbed at different wavelengths at this location. This provides spatially resolved information on the chemistry of the sample. Hyperspectral imaging has been used to perform a variety of different types of quality control of fish (Sun, 2010; Cheng & Sun, 2014), such as identification and quantification of blood (Skjelvareid et al., 2017), quantification of fat and water (Elmasry & Wold, 2008; Zhu et al., 2014), estimation of freshness (Nilsen et al., 2002; Mushy Halibut Syndrome, 2011), and freezing and thawing history (Zhu et al., 2013; Washburn et al., 2017; Anderssen et al., 2020). Recently, the HSI technology has transitioned from the research lab to industry, and it is possible to purchase a commercial system dedicated to quality control of seafood. In this study, we apply HSI to provide an estimate of fat and water composition of the samples.

Another characterization technique used to investigate the syndrome is diffusion tensor imaging (DTI), a specialized type of magnetic resonance imaging (MRI) (Basser, 1995). This technique was originally developed for the identification of brain disease and trauma and has recently been adapted for investigating structure in meat and seafood (Anderssen et al., 2022). DTI measures the restriction of water molecule diffusion in order to characterize the tissue environment. In bulk water, diffusion is isotropic, with molecules moving randomly in every direction. However, inside nerve or muscle cells, diffusion of water molecules is restricted due to the presence of the cell structure. As the cells have an elongated shape, water molecules are able to diffuse farther in some directions than others until they are obstructed by the cell membrane, hence diffusion is anisotropic. DTI makes measurements of the diffusion coefficient in multiple directions in order to measure this anisotropy, creating the diffusion tensor. This diffusion tensor has several metrics that describe the anisotropy, shown Fig. 1.

Fractional anisotropy (FA) tells how anisotropic the diffusion of water molecules in a pixel is and ranges on a scale from 0 to 1. Zero corresponds to completely isotropic diffusion, while one corresponds to diffusion restricted to along a single axis. Radial diffusivity (RD) describes the diffusivity along the narrowest axis of the diffusion tensor. Axial diffusion (AD) describes the diffusivity along the longest axis of the diffusion tensor. In addition, the mean diffusivity (MD) is measured, which describes the average diffusivity in the pixel without regards to orientation. Histology, hyperspectral imaging and diffusion tensor imaging were selected for this study because, when performed together, they enable evaluation of both the chemical and structural composition of the tissue in the vasskveite.

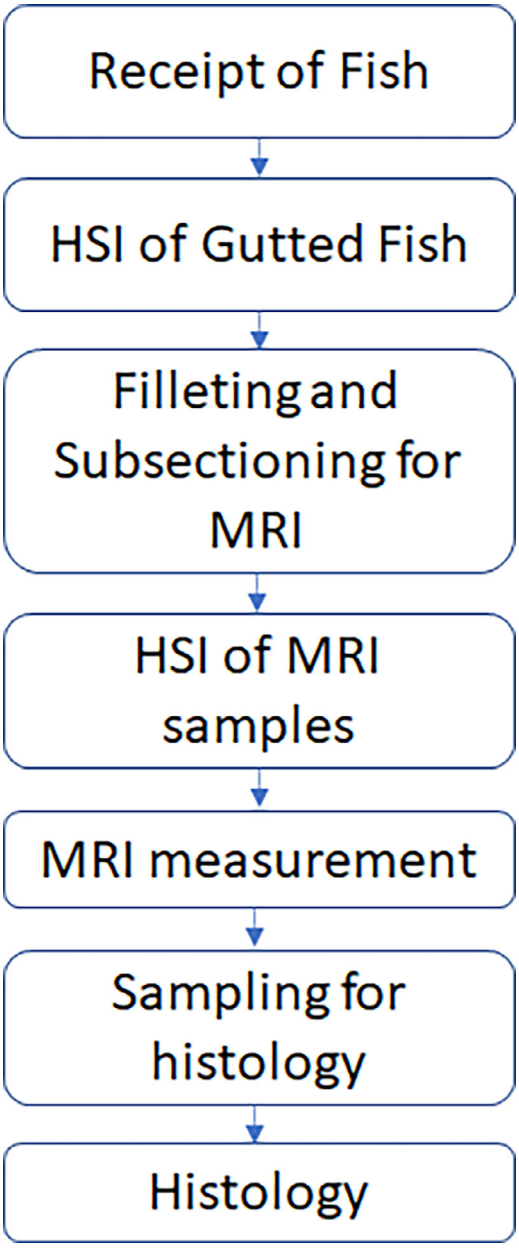

Fig. 2. Workflow of the characterization measurements performed during this study.

2. Materials and methods

2.1. Samples

Sixteen Greenland halibut *(Reinhardtius hippoglossoides)* were provided by Henry Johansen Drift AS, (Vengsøya, Norway). The fish originated from a commercial landing. At delivery, the fish were sorted into normal fish and vasskveite by trained personnel at Henry Johansen Drift. Eight examples of healthy halibut and eight examples of afflicted halibut were sent to Nofima. Fish were received at Nofima having been gutted, but not filleted nor the head removed. The workflow, shown Fig. 2, is as follows: Fish were scanned using HSI on both the ocular and the blind sides. Fish were then filleted and scanned again using HSI. For the measurements in this paper, small subsections (19g ± 3g) were then taken from the loin of the fish and vacuumed packaged. These subsections were scanned by HSI. Although samples were scanned multiple times using HSI, only the data from the subsections for MRI (16 images) were analyzed here in this paper. Samples were then measured via DTI MRI. After MRI measurement, further subsections were taken and sent for histology analysis.

2.2. Hyperspectral acquisition

There exist different types of acquisition modes of hyperspectral imaging, such as transmission, diffuse reflectance, and interactance. For this study, the interactance acquisition mode was used. Here, a strong illumination source is shone upon the sample and a camera that is offset a small distance measures the scattered light. Unlike diffuse reflectance, which only measures light reflected from the surface, interactance measures deeper into the sample, as multiple scattering events are required for the light to reach the camera. A schematic of the HSI setup is shown in Fig. 3. Dual illumination is used, as previous work has shown that two parallel light lines improve signal to noise compared to a single illumination source and avoids the problem of being unable to obtain a signal at sample edges (Sivertsen et al., 2009; Wold et al., 2006). The camera line is placed between the two light lines. The illumination source was a pair of custom-built fiber optics (Fiberoptics Technology Inc. Connecticut, USA). These were fitted with custom made collimating lenses (Optec S.P.A., Milano, Italy). Each light line contains six fiber optic bundles with each fiber optic fed by a 150W halogen lamp focused with an aluminum reflector (International Light Technologies, Massachusetts, USA, model L1090). The light lines are each approximately 400 mm long and 5 mm in width, and together have a total of 1800W of electrical input power.

The hyperspectral camera used for this study was the HySpex VNIR-1024 (Norsk Elektro Optikk, Oslo, Norway). The hyperspectral camera field of view is 0.56 mm x 300 mm with a pixel size of 0.28 mm x 0.28 mm. Light is measured in the 410–990 nm spectral region with approximately a 2.6 nm spectral resolution (216 bands). Samples were imaged on a conveyor belt traveling at 20 cm/s, a rate that conforms to the industrial production capacity limit of approximately one fillet per second. The hyperspectral camera operates in pushbroom mode, scanning the sample line by line at 714 frames per second as it moves through the field of view. The successive frames $F(\lambda, x)$ are stored as a hyperspectral image $R_i(\lambda, x, y)$.

2.3. MRI procedures

MRI images were acquired using a preclinical 7 Tesla MR Scanner (MRS*DRYMAG, MR solutions, Guildford, UK) using a mouse quadrature coil. Diffusion tensor images were taken using a Fast Spin Echo sequence. TR was 6 s, TE was 35 ms and diffusion was measured in 10 sampling directions. The b value was 800 s/mm2, in-plane resolution is 310 microns by 310 microns, slice thickness was 1 mm and number of slices was 60. Total measurement time was approximately 20 min.

2.4. Histology

Thin subsections (1-2 mm) were taken from the samples after MRI scanning. The subsections were placed in formalin for two days before being transferred to a 70% ethanol solution. Samples were then sent to Norwegian Veterinary Institute for analysis. Slices of the subsections were taken, fixed, and stained with hematoxylin and eosin (H&E). This stains the cytoplasm of the muscle fibers pink while the connective tissue is highlighted in blue. Fat will not take up these dyes. The staining was done on deparaffinized sections, the process is 2 × 5 min in xylene,

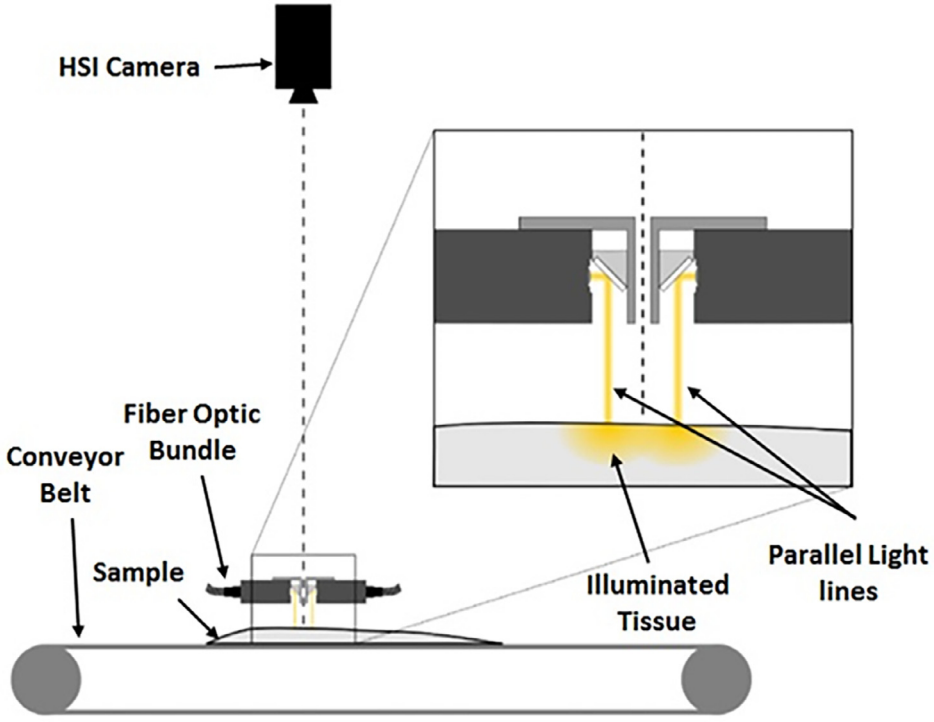

Fig. 3. Schematic of the hyperspectral interactance imaging setup.

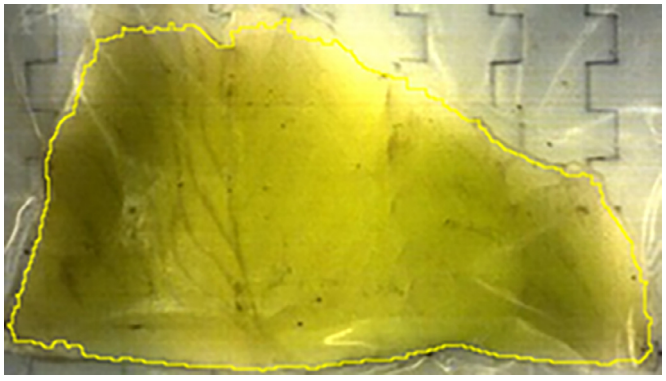

Fig. 4. Example of segmentation (yellow line) between tissue and the conveyor belt on an image reconstructed by selecting wavelengths in the RGB spectral regions.

rehydration in a series of ethanol (2 × 100; 2 × 95; 1 × 90; 1 × 70%) and rinsing with dH_2O. One section from each fish, i.e., six sections from each fish group were stained with H&E (Fisher, Fair Lawn, NJ), dehydrated in the alcohol series back to xylene and mounted in quick hardening mounting medium Tissue-Tek Film Sakura (Sakura Finetek Nagano, Nagano, Japan). The slides were scanned with a Nanozoomer S360 Hamamatsu. The images were evaluated by visual inspection.

2.5. Image analysis

2.5.1. HSI analysis

Analysis of hyperspectral data was performed using the specialized software Breeze (Prediktera AB, Umeå, Sweden). In order to correct for changes in camera sensitivity and illumination with time, a calibration sample of Teflon, which has stable optical properties (Tsai, 2008), is measured before each set. The calibration sample used is a square 300 mm on each side with a thickness of 25 mm. One hundred successive frames of the Teflon target are averaged together to calculate a reference frame $R_a(\lambda, x)$. The absorption of the interactance images is then calibrated as $I(\lambda, x, y) = -\ln(R_i(\lambda, x, y)/R_a(\lambda, x))$, where $R_i(\lambda, x, y)$ is the hyperspectral image of the packaged fillet section. After calibration, segmentation was performed to identify which pixels in the hyperspectral image correspond to either the fish sample or the conveyor belt. Fig. 4 shows an example of a segmented hyperspectral image.

Once images were segmented, the pixels corresponding to fish fillets were analyzed using constrained spectral unmixing (Skjelvareid et al., 2017). In linear mixing models, the measured spectrum in a pixel is assumed to be the additive of sum of the spectra of the constituents (e.g., fat, water, blood) in that pixel, example shown Fig. 5. Therefore, by finding the linear combination of end-member spectra that best fit the measured spectrum, the composition can be determined. For the halibut, the spectra were analyzed using water, fat, and blood (oxyHb, deoxyHb, and metHb) endmembers in order to estimate the relative amount of these constituents. The difference between the measured signal and the reconstructed signal was minimized by using a non-negative least squares regression. A first order polynomial was included to correct for offset and slope (Skjelvareid et al., 2017). Note, the analysis here only finds the relative abundances of the two constituents in the signal and is not converted to the actual percentages of fat and water in the tissue. After all the spectra in a hyperspectral image were converted into relative abundances, the average for all the pixels was taken to give a single estimated value of each constituent for the sample.

2.5.2. MRI processing

After acquisition, images were converted from the dicom format to Nifti format, the b-table calculated, and the diffusion tensor images of the FA, RD, AD and MD metrics were created using DSI studio (Yeh, 2021). Reconstruction of the fiber tractography was performed according to the methods laid out in Yeh et al. (2013).

2.5.3. MRI statistical analysis

Statistical analysis was performed on all the FA, RD, and AD images from each sample in Python (Python Software Foundation, Delaware, USA). For each sample, the DTI metrics of each pixel were compiled from every image slice into a single matrix. Note, as the values of FA, RD, and AD outside the sample in the image are zero, these values were discarded for analysis. The distribution of the DTI metrics was plotted as histograms and the average and standard deviation of each metric for each sample was calculated. Tests for significance were performed using the students t-test (Student, 1908). Significance level was taken to be $p < 0.05$.

For the tractography results, the average curl was calculated for each sample, correcting for the anisotropy between the in-plane and slice resolution. The curl of a fiber is the ratio of its length to the distance between its end points. A low value indicates the fibers are mostly straight, while a high value of curl indicates a wavy or looped form.

3. Results

3.1. Hyperspectral imaging

The relative abundances of fat and water in the hyperspectral signal showed a clear distinction between the groups, shown Fig. 6. The average abundance of fat in the signal for the healthy samples was 6.9e-3 (± 9.0e-4) while it was only 4.3e-3 (± 1.2e-3) in the vasskveite samples.

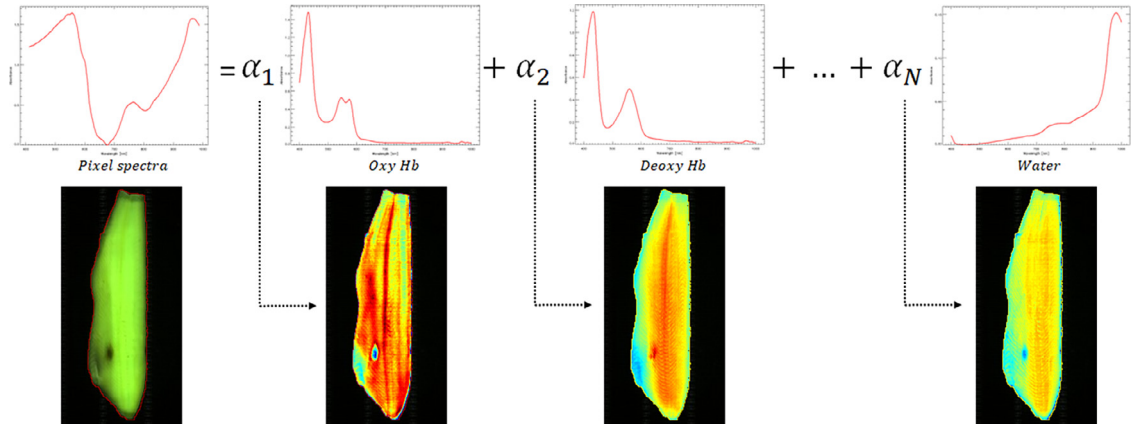

Fig. 5. Example of spectral unmixing for a single pixel from a hyperspectral image.

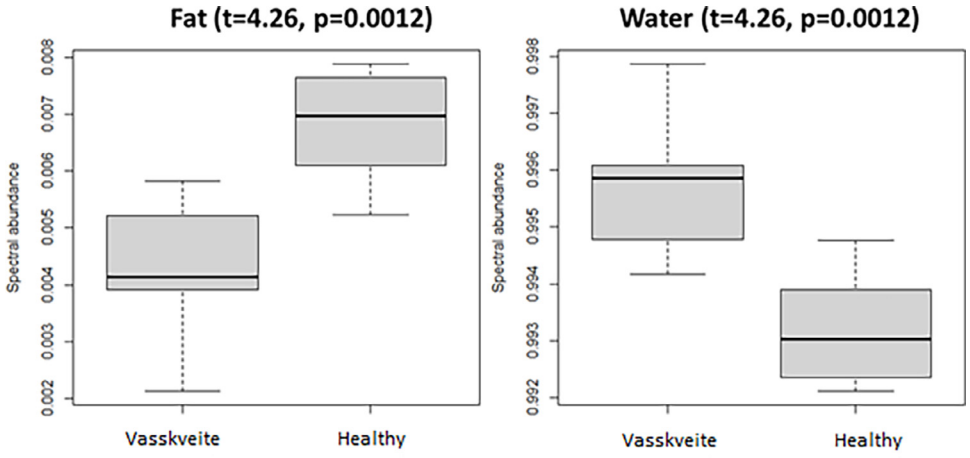

Fig. 6. Box and whiskers plot of the average spectral abundances for fat and water in the healthy and vasskveite samples.

Similarly, the average abundance of water in the signal of the healthy halibut was 0.993 (± 0.0009) and 0.0996 (± 0.0012) in the vasskveite ($t = 4.26$, $p = 0.0012$).

3.2. Magnetic resonance imaging

The DTI images show distinct differences between the healthy and the vasskveite samples, example shown Fig. 7. The AD and MD images are very similar in appearance to the RD image and therefore are not shown. In the images, the brighter the pixel, the higher the FA or RD value for that location. Several differences are immediately noticeable. In the healthy samples, the muscle structure is identifiable, with higher FA values and lower RD values between the segments. In contrast, individual muscle segments are not identifiable in the images of the vasskveite samples, which display a fairly uniform texture. More generally, the FA images were darker, indicating lower anisotropy in the tissue, while the RD, MD and AD images were brighter, indicating higher values.

Due to the large number of images from each sample, visual inspection alone cannot give a thorough analysis of the results. Therefore, we histogram the data in order to get a better overview of the difference between the two types of samples, Fig. 8.

The average DTI metrics for the are presented in Table 1. Clear differences are seen between the results for the healthy and vasskveite samples and the t-test produces statistically significant differences for all metrics. The results indicate that the vasskveite muscle fibers are larger and less constricted than in healthy fish. The lower FA value for the vasskveite indicates the average shape of muscle fiber in afflicted fish is more isotropic than in healthy fish. The MD DTI metric describes the overall diffusion constant of water molecules in the muscle fibers. It is without respect to orientation, such that it is the coefficient of diffusion averaged over all directions in the muscle fiber. The higher value suggests that diffusion is less restricted in the muscle cells of afflicted fish and therefore the average size of the muscle cells is larger. This interpretation is supported by the higher values of AD and RD in afflicted fish, as diffusion is less restricted both parallel and perpendicular to the main axis of the muscle cell than compared to healthy fish.

Examples of tractography for the healthy and vasskveite are shown in Fig. 9a and 9b, respectively. Tractography converts the measured diffusion coefficients in the MRI image into the muscle fiber structure in the sample. Muscle fibers are depicted as the thin tubes in the images. The fiber direction is color coded, such that the color of a fiber changes as its orientation changes along its length. Overall, the muscle fiber structure in the healthy sample shows a highly parallel structure. This is what is typically seen in healthy muscle tissue. In contrast, the vasskveite shows fibers in many different directions, in some cases looping back on themselves. This is reflected in the high curl values for the vasskveite samples. The average curl for the vasskveite samples was 2.60 ± 0.71 while the healthy samples only had an average of 1.80 ± 0.24 (2.84, $p = 0.023$). Due to this being the first use of tractography in food science, there are no other values in the literature for comparison.

3.3. Histology

Results between the healthy and vasskveite samples showed several clear differences, shown Fig. 10a and 10b, respectively. Due to the very soft nature of the tissue, taking samples of the vasskveite for histology was problematic. The tissue tended to fall apart under sampling instead of slicing neatly. This resulted in samples that are suitable for qualitative analysis but due to uncertainty around how much structural differences are intrinsic to the samples and how much arises from sampling difficulties, quantitative images analysis of the results was not attempted.

Visually, there are several notable differences with the vasskveite samples. Firstly, the tissue contains much less fat than the healthy samples, which are the white spherical features in the images. In the healthy samples, fat is clustered around the myocommata, the connective tissue between muscle segments, highlighted in blue. This is greatly decreased or absent in the vasskveite samples. Secondly, the fiber structure is disordered and somewhat more fragmented. While the healthy samples show muscle fibers with a neat, parallel structure, the fiber structure in the vasskveite samples shows a lack of orientation, with muscle cells that are both parallel and perpendicular to the sampling direction. This is witnessed by the combination of both round and oblong cell shapes in the tissue slices of afflicted fish. Cell shape in general is less regular in the vasskveite samples.

Table 1
Average FA, MD, AD and RD values for healthy and afflicted fish and the statistical significance between them.

Sample Type	FA (5.2, $p < 0.001$)	MD (-5.58, $p < 0.001$),	AD (-4.59, $p < 0.001$)	RD (-6.04, $p < 0.001$)
Healthy	0.25 ± 0.15	1.01 ± 0.30	1.24 ± 0.36	0.89 ± 0.29
Vasskveite	0.17 ± 0.09	1.29 ± 0.22	1.51 ± 0.26	1.18 ± 0.21

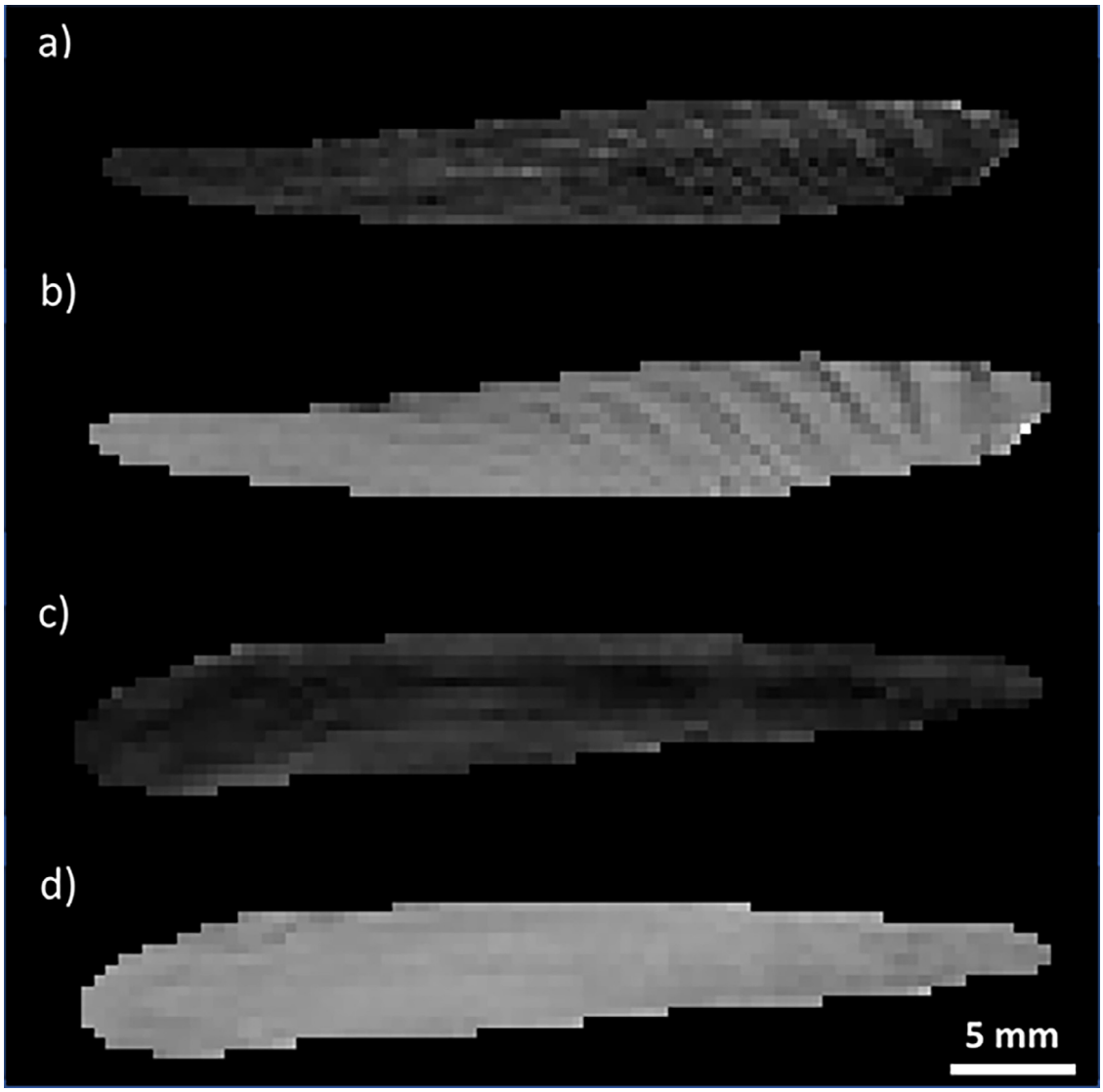

Fig. 7. Example DTI images (a) FA image of healthy sample (b) RD image of a healthy sample (c) FA image of a vasskveite sample (d) RD image of a vasskveite sample.

4. Discussion

All the different analysis techniques produce a consist picture for vasskveite: the tissue is structurally disordered and too low in fat. A surprising result was that the histology indicated that there did not seem to be any major difference in the amount of connective tissue between the muscle fibers for the healthy and vasskveite. There also was no clear difference in the degradation of the endomysium, the connective tissue between muscle fibers.

Several notable differences exist in the DTI metrics between the healthy and vasskveite samples. For the vasskveite, the main peak of the FA histogram is shifted to a lower value. This indicates less restriction and anisotropy in the tissue, suggesting disorder and a breakdown of the cell structure. Interestingly, for the vasskveite samples, the breakdown in tissue does not appear to be uniform. In general, the FA values in the center of the samples were lower than those on the edge of the sample. Similarly, the AD, MD and RD are all shifted to higher values compared to the healthy fish and show a similar distribution. The DTI tractography and histology also supports this, both showing fiber orientations in many different directions. In addition, the healthy fish contain striations of higher FA and lower AD, RD, and MD between the tissue segments. Evaluation of both the images and histograms of the vasskveite halibut does not show this effect. There are two possible causes here. Firstly, this may arise from highly restricted diffusion of water inside connective tissue. Secondly, medical research indicates that the presence of fat can lead to higher fractional anisotropy (Williams et al., 2013). Based on the histological images, the healthy individuals showed fat clustered along the connective tissue between muscle segments. For the vasskveite samples, connective tissue did not appear degraded in the histological images. Therefore, we believe the fat is the dominant source of the high FA values in the halibut images. However, in order to definitively separate out the two constituents, the standard DTI sequence is not sufficient and future studies using higher dimensionality DTI sequences, such as T_2-DTI and T_1-T_2-DTI (de Almedia Martins et al., 2020) will be tested in order to produce resolution between fat and water in the samples.

Using tractography to evaluate tissue in food science is a novel application and these results show it is promising as a technique to provide more information on muscle fiber structure. Future studies are planned to perform quantitative correlation between histology and DTI results to confirm agreement between the two techniques. Provided the two techniques produce similar results, DTI tractography has several advan-

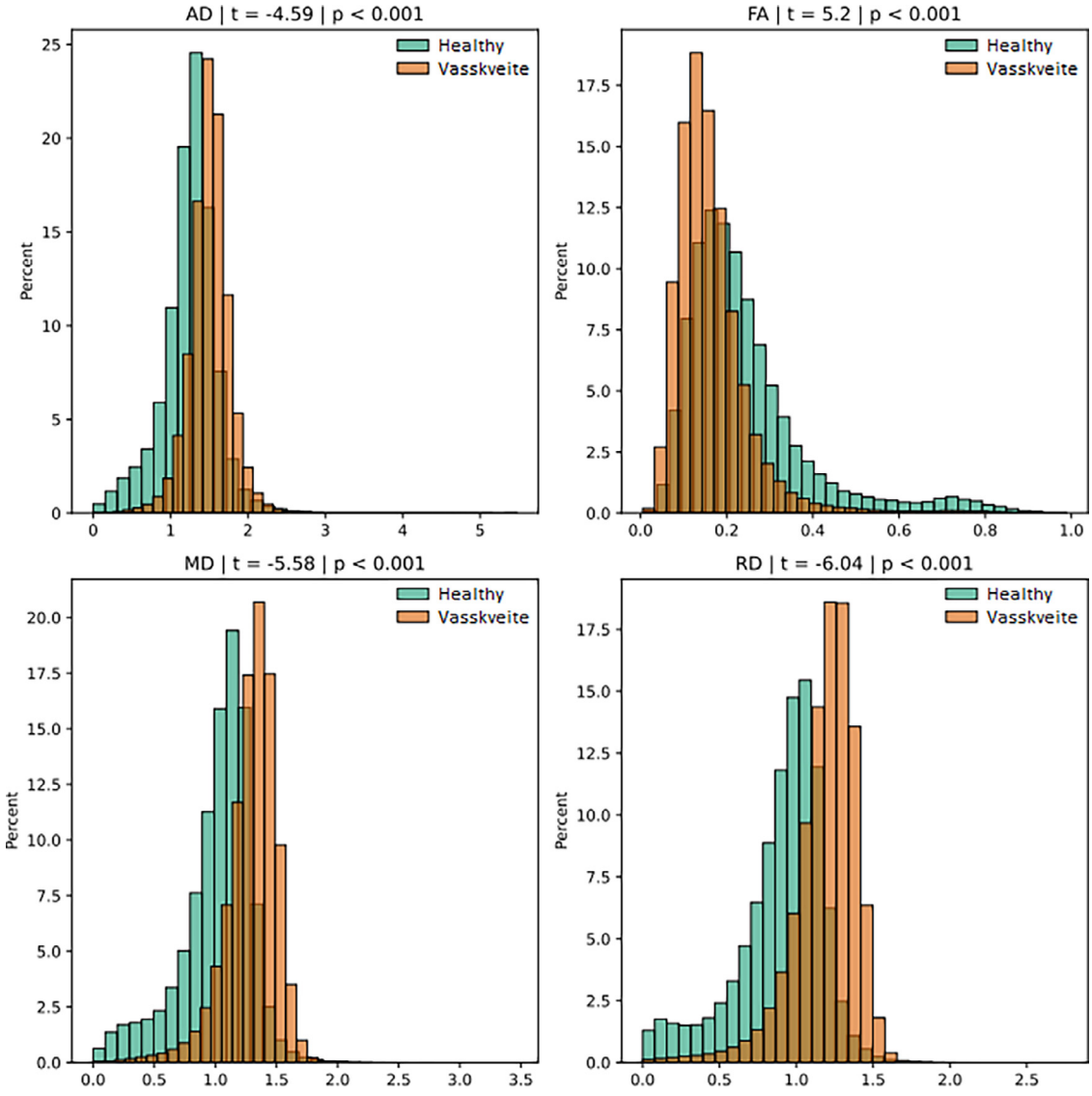

Fig. 8. Histograms of AD, FA, MD and RD values for healthy and vasskveite samples.

tages over histology. The method can provide information much more quickly, is possible to perform over larger areas, provides information in three dimensions and is non-invasive, such that repeated measurements can be made on samples to track changes during processing or storage.

The lack of fat in the tissue of poor-quality halibut is consistent with the theory that the soft texture stems from a nutritional deficiency in the halibut's diet. Similar findings have been reported for other fish species. Starvation of winter flounder resulted in a reduced hypodermal lipid layer, higher water content and atrophy of the white muscle fibers (Maddock & Burton, 1994). Further research is necessary to determine whether the low-fat content itself is the cause of the soft tissue or whether it is a side effect of another underlying issue. For example, previous findings have shown that pre-slaughter stress affected Atlantic salmon muscle quality through acceleration of enzymatic muscle degradation (Bahuaud et al., 2010).

While it is useful to understand that the jelly-like consistency of the tissue likely stems from nutritional deficiencies, this is a problem that is difficult to remedy. It is unlikely modifying capture or slaughter procedures will have much of an effect to prevent the fish from developing the mushy texture, for example. However, the correlation of low-fat content in tissue with the vasskveite syndrome at least provides an avenue for rapid screening right after capture. There currently exist commercial HSI systems for use in fish processing plants that can provide quantification of fat and water content in real time. Characterization can be performed on every fish from a landing. This process is automated, such that there is no need for human intervention in the procedure and equipment can be installed above existing conveyor belts in the processing plant. Measurements taken on gutted fish found that despite the thick skin of the halibut, the light is able to penetrate down to the underlying muscle. As such, the technique can be used on fish right after capture. By quantifying the amount of fat and water in each fish, machine learning can be applied to automatically classify fish with too low of fat content as afflicted with vasskveite syndrome. These fish can then be removed from a delivery even before they start to develop the undesirable jelly-like texture. Vasskveite can be used in lower value products, such as fish feed or silage, while the healthy fish can be directed to higher value product lines, such as smoking or curing (ElMasry et al., 2012). This solution would enable both exporters and purchasers to have better confidence in product quality and help minimize complaints and returns. Future studies will include chemical analysis to confirm the relationship between low fat and the soft tissue, as well as measurements immediately after slaughter to confirm the ability to predict the syndrome before rigor mortis.

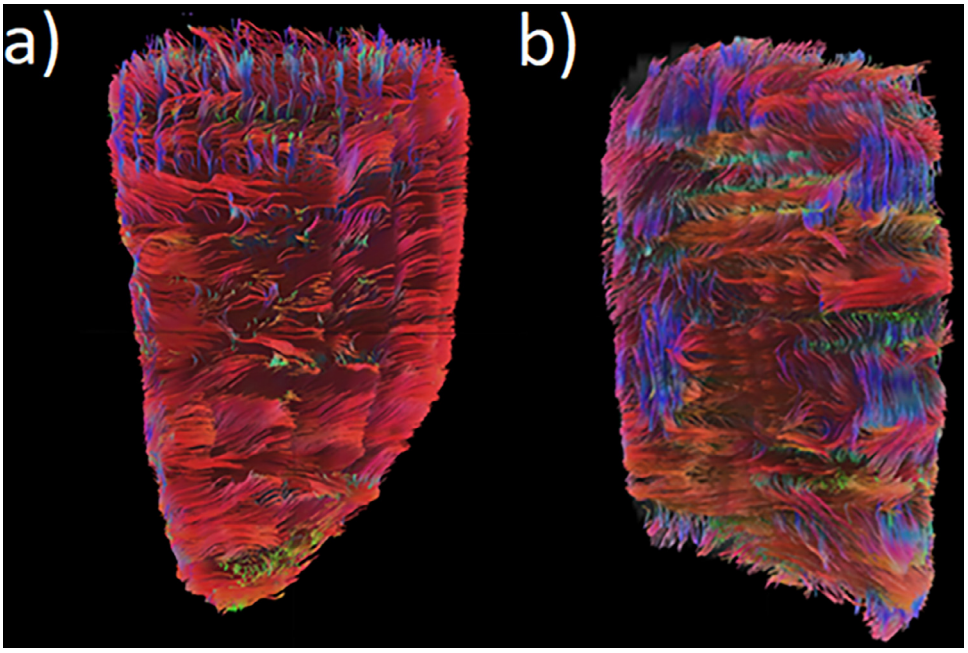

Fig. 9. Example tractography images for (a) healthy halibut (b) vasskveite.

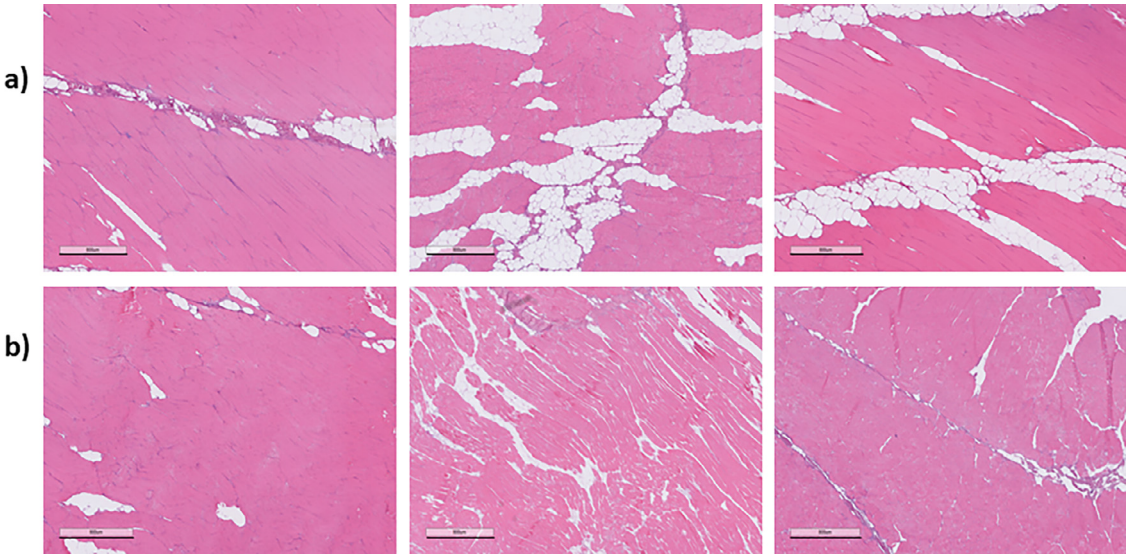

Fig. 10. Three example histology images for (a) healthy tissue and (b) vasskveite tissue. Muscle fibers are stained red, connective tissue is blue and fat is unstained. Scalebars represents 800 mm.

5. Conclusions

The vasskveite syndrome appears to arise from disordered tissue growth and a lack of fat in the muscle. Histology and diffusion tensor imaging (DTI) tractography indicates a loss of the usual, highly parallel structure in the muscle fibers. Hyperspectral imaging (HSI), histology and DTI fraction anisotropy (FA) values all indicate lower fat content in the vasskveite. Examination of DTI FA images and histology indicate this effect seems to be most prominent in loss of fat around the connective tissue between muscle segments. Degradation of connective tissue was not observed. The exact cause of these effects is still uncertain, but the results support the theory that the syndrome arises from dietary deficiencies in the halibut. Hyperspectral imaging looks to be a potential solution for rapidly screening halibut for the syndrome after landing to prevent the sale of inferior quality fish.

Ethical statement

All fish samples for the study were obtained from a commercial supplier.

Declaration of Competing Interest

The authors have no affiliation with any organization with a direct or indirect financial interest in the subject matter discussed in the manuscript.

Data availability

Data will be made available on request.

Acknowledgments

This project is supported by NFR funding grant 294805 and is also part of Digifoods, a Norwegian Strategic Research Initiative (project number 309259). The authors thank Gunhild Johanssen for assistance with the histology sampling. The authors thank the PETcore facility at UiT for the use of the preclinical MRI scanner.

References

Anderssen, K. E., Kranz, M., Syed, S., & Stormo, S. (2022). Diffusion tensor imaging for spatially-resolved characterization of muscle fiber structure in seafood. *Food Chemistry, 380*, Article 132099. 10.1016/j.foodchem.2022.132099.

Anderssen, K. E., Stormo, S. K., Skåra, T., Skjelvareid, M. H., & Heia, K. (2020). Predicting liquid loss of frozen and thawed cod from hyperspectral imaging. *LWT, 133*, Article 110093. 10.1016/j.lwt.2020.110093.

Basser, P. J. (1995). Inferring microstructural features and the physiological state of tissues from diffusion-weighted images. *NMR in Biomedicine, 8*, 333–344. 10.1002/nbm.1940080707.

Bahuaud, D., Mørkøre, T., Østbye, T. K., Veiseth-Kent, E., Thomassen, M. S., & Ofstad, R. (2010). Muscle structure responses and lysosomal cathepsins B and L in farmed Atlantic salmon (Salmo salar L.) pre- and post-rigor fillets exposed to short and long-term crowding stress. *Food Chemistry, 118*, 602–615. 10.1016/j.foodchem.2009.05.028.

Capture production by species, fishing areas and countries or areas, (2017) retrieved from: https://www.fao.org/fishery/static/Yearbook/YB2017_USBcard/root/capture/b31.pdf.

Cheng, J. H., & Sun, D. W. (2014). Hyperspectral imaging as an effective tool for quality analysis and control of fish and other seafoods: Current research and potential applications. *Trends in Food Science and Technology, 37*, 78–91. 10.1016/j.tifs.2014.03.006.

de Almedia Martins, J. P., Tax, C. M. W., Reymbaut, A., Szczepankiewicz, F., Chamberland, M., & Jones, D. K. (2020). Computing and visualising intra-voxel orientation-specific relaxation–diffusion features in the human brain. *Human Brain Mapping, 42*, 310–328. 10.1002/hbm.25224.

ElMasry, G., & Wold, J. P. (2008). High-speed assessment of fat and water content distribution in fish fillets using online imaging spectroscopy. *Journal of Agricultural and Food Chemistry, 56*, 7672–7677. 10.1021/jf801074s.

ElMasry, G., Barbin, D. F., Sun, D. W., & Allen, P. (2012). Meat quality evaluation by hyperspectral imaging technique: an overview. *Critical Reviews in Food Science and Nutrition, 52*, 689–711. 10.1080/10408398.2010.507908.

Kvile, K. "Forskerne har analysert ti blåkveiter uten å finne svar på hvorfor den er så vassen" (March 11, 2019) referenced from: https://www.fiskeribladet.no/tekfisk/forskerne-har-analysert-ti-blakveiter-uten-a-finne-svar-pa-hvorfor-den-er-sa-vassen/2-1-561784.

Maddock, D. M., & Burton, M. P. M. (1994). Some effects of starvation on the lipid and skeletal muscle layers of the winter flounder, pleuronectes americanus. *Canadian Journal of Zoology, 72*, 1–8. 10.1139/z94-223.

Mushy Halibut Syndrome, Diseases of Wild and Cultured Fishes in Alaska, (2011), State of Alaska's Fish Pathology Lab, retrieved from: http://www.adfg.alaska.gov/static/species/disease/pdfs/fishdiseases/mushy_halibut_syndrome.pdf.

Nilsen, H., Esaiassen, M., Heia, K., & Sigernes, F. (2002). Visible/near-infrared spectroscopy: a new tool for the evaluation of fish freshness? *Journal of Food Science, 67*, 1821–1826. 10.1111/j.1365-2621.2002.tb08729.x.

Sandøy, Ø. "Ulukka er at det er så godt som umogleg å skilje ut vasskveita frå fangsten" (February 25, 2019) referenced from: https://www.fiskeribladet.no/meninger/-ulukka-er-at-det-er-sa-godt-som-umogleg-a-skilje-ut-vasskveita-fra-fangsten/8-1-65458.

Sivertsen, A. H., Chu, C.-K., Wang, L.-C., Godtliebsen, F., Heia, K., & Nilsen, H. (2009). Ridge detection with application to automatic fish fillet inspection. *J. Food Eng., 90*, 317–324. 10.1016/j.jfoodeng.2008.06.035.

Skjelvareid, M. H., Heia, K., Olsen, S. H., & Stormo, S. K. (2017). Detection of blood in fish muscle by constrained spectral unmixing of hyperspectral images. *Journal of Food Engineering, 212*, 252–261. 10.1016/j.jfoodeng.2017.05.029.

Student. (1908). The probable error of a mean. *Biometrika, 6*, 1–25.

Sun, D. W. (2010). *Hyperspectral imaging for food quality analysis and control*. Elsevier.

Tsai, B.K., Allen, D.W., Hanssen, L.M., Wilthan, B., Zeng, J., (2008) A comparison of optical properties between solid PTFE (Teflon) and (low density) sintered PTFE, Proc. SPIE 7065, Reflection, Scattering, and Diffraction from Surfaces, 70650Y 10.1117/12.798138.

Washburn, K. E., Stormo, S. K, Skjelvareid, M. H., & Heia, K. (2017). Non-invasive assessment of packaged cod freeze-thaw history by hyperspectral imaging. *Journal of Food Engineering, 205*, 64–73. 10.1016/j.jfoodeng.2017.02.025.

Williams, S. E., Heemskerk, A. M, Welch, B., Li, K., & Damon, B. M. (2013). Quantitative effects of inclusion of fat on muscle diffusion tensor MRI measurements. *Journal of Magnetic Resonance Imaging, 38*, 1292–1297. 10.1002/jmri.24045.

Wold, J. P., Johansen, I. R., Haugholt, K. H., Tschudi, J., Thielemann, J., Segtnan, V. H., … Wold, E. (2006). Non-contact transflectance near infrared imaging for representative on-line sampling of dried salted coalfish (bacalao). *J. of near Infrared Spectroscopy, 14*(1), 59–66.

Yeh, F. C., Verstynen, T. D., Wang, Y., Fernandez-Miranda, J. C., & Tseng, W. Y. I. (2013). Deterministic diffusion fiber tracking improved by quantitative anisotropy. *PLOS One*. 10.1371/journal.pone.0080713.

Yeh, F.C. (2021, May 15). DSI studio (Version 2021 May). Zenodo. 10.5281/zenodo.4764264).

Zhu, F., Zhang, D., He, Y., Liu, F., & Sun, D. W. (2013). Application of visible and near infrared hyperspectral imaging to differentiate between fresh and frozen–thawed fish fillets. *Food and Bioprocess Technology, 6*, 2931–2937. 10.1007/s11947-012-0825-6.

Zhu, F., Zhang, H., Shao, Y., He, Y., & Ngadi, M. (2014). Mapping of fat and moisture distribution in atlantic salmon using near-infrared hyperspectral imaging. *Food and Bioprocess Technology, 7*, 1208–1214. 10.1007/s11947-013-1228-z.